Simulation of Gymnastics Performance Based on MEMS Sensor

Bingxin Chen (chenbingxin15@163.com)
College of Physical Education Hunan Normal University
Lifei Kuang
College of Physical Education Hunan Normal University
Wei He
College of Physical Education Hunan Normal University

Research

Keywords: MEMS Sensor, Gymnastics Performance, Motion Capture, Inertial Measurement Unit

Posted Date: May 19th, 2021

DOI: https://doi.org/10.21203/rs.3.rs-470739/v1

Version of Record: A version of this preprint was published at EURASIP Journal on Advances in Signal Processing on July 26th, 2021. See the published version at https://doi.org/10.1186/s13634-021-00760-4.

Simulation of Gymnastics Performance Based on MEMS Sensor

Bingxin Chen[1, a*], Lifei Kuang[1, b*] and Wei He[2, c]

[1]*College of Physical Education Hunan Normal University, Changsha 410000, Hunan, China*

[2]*Department of Physical Education Changsha Normal University, Changsha 410000, Hunan, China*

[a]*E-mail: chenbingxin15@163.com*

[b]*E-mail: lifekuang1@163.com*

[c]*E-mail: ccsbb@163.com*

[*]*Corresponding author*

Abstract: The development and progress of multi-sensor data fusion theory and method also lay the foundation for the research of human posture tracking system based on inertial sensor. This paper mainly studies the simulation of gymnastic performance based on MEMS sensors. In the preprocessing of reducing noise interference, this paper mainly uses median filter to remove signal burr. In this paper, the use of virtual character model for gymnastics performance. The computer receives sensor data from the sink node of the motion capture device through a Bluetooth communication module. The unit calculates the quaternion output from the dynamic link library of sensor data processing, calculates the rotation and coordinate offset of the limb where each sensor node is located, and realizes the real-time rendering of the virtual human model by using the driver of the human model. At the same time, it controls the storage of sensor data, the driving of model and the display of graphical interface. When the gesture action is about to happen, a trigger signal is given to the system to mark the beginning of the action, so as to obtain the initial data of each axis signal of MEMS sensor. When the gesture action is completed, a signal to end the action is given to the system to mark the end of the action, so that the original signal data between the beginning and end of the gesture action can be captured. In order to ensure the normal communication between PS and PL, it is necessary to test the key interface. Because the data received by the SPI acquisition module is irregular, it is unable to verify whether the data is wrong. Therefore, the SPI acquisition module is replaced with an automatic incremental data module, and it is generated into an IP core to build a test platform for testing. The data show that the average measurement errors of x-axis displacement, Y-axis displacement, z-axis displacement and three-dimensional displacement are 8.17%, 7.51%, 9.72% and 8.7%, respectively. The results show that the MEMS sensor can accurately identify the action with high accuracy.

Keywords: MEMS Sensor, Gymnastics Performance, Motion Capture, Inertial Measurement Unit

1. Introduction

At present, new forms of human-computer interaction terminals such as mobile Internet, cloud computing and Internet of things, such as smart clothing, smart accessories and other wearable computing systems, have become fashionable consumer electronic products. In addition, the cross integration of wearable computing and emotional computing, physiological computing and social computing will enrich the research content in the fields of big data, human-computer interaction and intelligent sensing; the in-depth application of wearable computing in the fields of health care, digital media, mobile communication, textile and clothing will also bring new industrial chain. The basic gymnastic movements have gradually evolved from simple to complex, which makes people's pursuit of gymnastic artistry more and more intense, and the aesthetic orientation tends to be diversified. From the initial simple and complex cultural system, people's aesthetic orientation tends to be diversified,

and the pursuit of artistry is more and more intense.

For the rapid acquisition of attitude information of integrated navigation, it can not meet the requirements to complete all the solutions on PC. a hardware platform is built to solve the attitude information. In fact, the calibration of motion attitude of MEMS inertial sensor motion capture system is to use inertial sensor to collect real-time motion data of human body, convert it into motion attitude data of three-dimensional human skeleton model established by the system, and then use human skeleton model to realize human action simulation.

The application of MEMS sensors in gymnastics performances has very good practical significance. K Józef proposed and verified a calibration method for three-dimensional acoustic vector sensor (AVS) for direction of arrival (DoA) estimation. The AVS device based on the p-p principle can be composed of a standard pressure sensor and a signal processing system. First, perform an amplitude calibration to compensate for the difference in amplitude between the pairs of microphones located on each axis. In order to verify the validity of the calibration method, he used a low-cost MEMS microphone and DSP board to construct a reference AVS. In order to verify the calibration method, he compared the accuracy of the calibration sensor with the commercial AVS and conducted a series of experiments. Although his research is innovative, there are some flaws in the verification process [1]. Kim Y discussed the stress caused by humidity saturation in MEMS sensor devices after temperature cycling. He characterized the material properties of the molding compound used for MEMS devices at wet, temperature and time. He used dynamic mechanical analysis (DMA) method to carry out a series of stress relaxation tests and obtained the viscoelastic properties of molding compound. He used the experimental data for numerical simulation, and estimated the temperature and humidity stress of MEMS sensor device under temperature cycle. Although his research is more accurate, but the lack of necessary experimental data [2]. Park DH studied the influence of the MEMS airbag sensor package module on the signal. In order to eliminate the impact of shell vibration, he introduced a new sensor package on the flexible circuit board, which was directly pasted on the surface of the frame structure with an adhesive. For the signal characteristics, impact tests were carried out on traditional sensor packaging and direct connection sensors using aluminum channels and car side frames. In order to understand the vibration effects of packaged components and structures, he also performed numerical analysis. Although he proved that the vibration characteristics of the frame structure and the module housing and the module installation position have a significant impact on the generation of shock signals, the content of numerical analysis is lacking [3]. Huang H believes that the dual-axis scanning mirror assembly (TSAY) is a key component of the optoelectronic system, which is usually used for precise positioning, tracking, scanning and stabilization of the line of sight (LOS). He designed and developed a TSAY prototype. In order to improve the control bandwidth, he optimized the structural topology of the TSAY elliptical mirror to reduce the moment of inertia while maintaining the surface flatness. He uses flexible hinges to achieve a wide range of angles. In order to suppress the angular disturbance caused by the linear vibration of the base, he constructed an adaptive feedforward loop with a base integrated microelectromechanical system (MEMS) accelerator to enhance the TSAY feedback loop. Although his research is relatively comprehensive, some of his expositions are not accurate enough [4].

In this paper, the random drift error of gyroscope sensor is analyzed, and the random drift error data modeling method based on time series model and the random drift error compensation method based on Kalman filter are carried out. The attitude of the processed sensor signal is calculated, and the attitude angle calculated by the angular velocity signal is fused with the attitude angle calculated by the

acceleration signal for correction. Finally, the attitude angle with higher accuracy is given.

2. Method

2.1 MEMS Sensor

The physical picture of MEMS sensor is shown as in Figure 1. STM32L151 is a microcontroller chip of STM32L151. The chip adopts high performance and ultra-low power 32-bit MCU with high performance arm cortex 3 RISC core. The operating frequency is between 32kHz and 32mhz. It integrates USB power supply, memory protection unit (MPU), high-speed embedded memory (512KB flash memory and 80kbram), and enhanced I / O and peripherals connected to two APB buses. The chip has excellent real-time performance, superior efficacy and maximum integration, which is suitable for wearable intelligent devices [5-6].

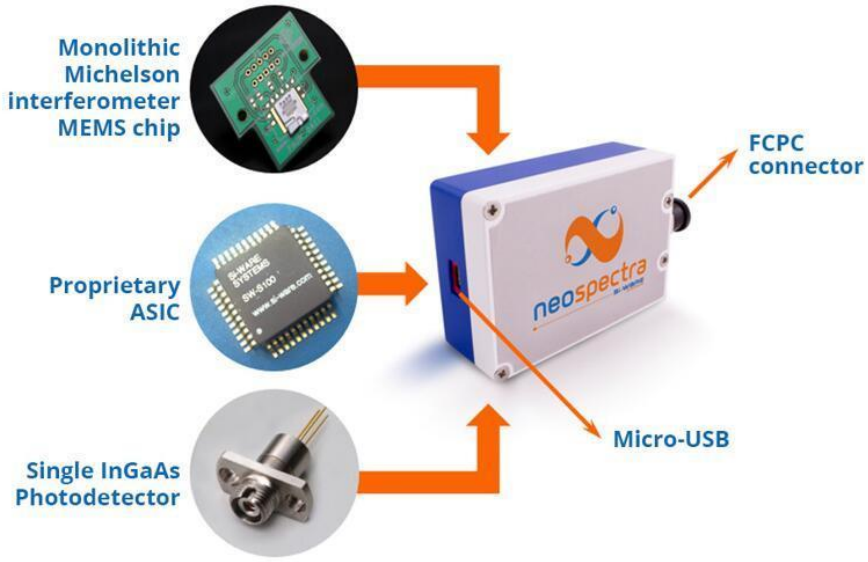

Figure 1. Physical image of MEMS sensor (picture from http://alturl.com/6ve7q)

Assuming that the probability density function at k-1 time is $p(x_{k-1}|Y_{k-1})$, $p(x_k|Y_{k-1})$ is obtained from $p(x_{k-1}|Y_{k-1})$, and the states x_k and Y_{k-1} are independent of each other [7].

$$p(x_k, x_{k-1}|Y_{k-1}) = p(x_k|x_{k-1}, Y_{k-1})p(x_{k-1}|Y_{k-1}) = p(x_k|x_{k-1})p(x_{k-1}|Y_{k-1}) \quad (1)$$

Integrate x_{k-1} to get the CK equation:

$$p(x_k|Y_{k-1}) = \int p(x_k|x_{k-1})p(x_{k-1}|Y_{k-1})dx_{k-1} \quad (2)$$

Where $p(x_k|x_{k-1})$ is the state transition probability, which is determined by the system state transition equation and including state noise [8].

Use Bayes' formula to update the prior probability density to obtain the posterior probability density, the expression is as follows [9]:

$$p(x_k|Y_k) = \frac{p(y_k|x_k, Y_{k-1})p(x_k|Y_{k-1})}{p(y_k|Y_{k-1})} \quad (3)$$

According to the observation equation, y_k is only related to x_k and noise, and the expression is as follows [10]:

$$p(x_k \mid Y_k) = \frac{p(y_k \mid x_k) p(x_k \mid Y_{k-1})}{p(y_k \mid Y_{k-1})} \quad (4)$$

In the formula, $p(y_k \mid Y_{k-1}) = \int p(y_k \mid x_k) p(x_{k-1} \mid Y_{k-1}) dx_k$, $p(y_k \mid x_k)$ is the likelihood probability, representing the current system state, and the similarity with the actual measured value, determined by the observation state equation, including observation noise [11].

When collecting data, factors such as whether the sensor is stable, where the sensor is worn and other factors have a certain relationship with the classification and recognition of gait. The sensor's wearing part is different, and the collected acceleration data is also different, so it will directly affect the effectiveness of recognition and classification. Acceleration sensors are often worn on the arms, wrists, waist, chest and other positions. Energy consumption also affects the size of the sensor power supply module and the overall module size. In addition, the data acquisition module must have sufficient memory space to store the collected data and related software programs [12-13].

Take three consecutive frames of human motion image sequence and mark them as k+1 frame, k frame and k-1 frame respectively. The frame difference method is calculated as [14]:

$$G(x, y) = \left[f_{k+1}(x, y) - f_k(x, y) \right] + \left[f_k(x, y) - f_{k-1}(x, y) \right] \quad (5)$$

$$H(x, y) = \begin{cases} 1 & \left| G(x, y) \right| > T \\ 0 & \left| G(x, y) \right| \le T \end{cases} \quad (6)$$

$$H(x, y) = \begin{cases} 1 & \mathrm{T1} \le \left| G(x, y) \right| \le T2 \\ 0 & others \end{cases} \quad (7)$$

In the formula, $G(x, y)$ is the three-frame difference image, $f_k(x, y)$ is the gray component of the human motion image sequence, and (x, y) is the position representation of the pixel [15].

Since the carrier interference magnetic field error has a greater impact on the accuracy of the magnetometer output, the error modeling is carried out for this error, and its expression is as follows [16]:

$$\Delta\psi = A + B\sin\psi_m + C\cos 2\psi_m + D\sin 2\psi_m + E\sin 2\psi_m \quad (8)$$

Among them, ψ_m is the heading output by the magnetometer, A is the circular deviation, and $B\sin\psi_m + C\cos 2\psi_m$ is the semicircular deviation [17].

2.2 Gymnastics Performance

Performance gymnastics is a kind of sports performance form that combines gymnastics elements and performing arts. It is a kind of sports culture art form that takes gymnastics elements as the basis, takes performance as the purpose, takes sports content as the performance material through artistic

performance means, and embodies sports culture. In addition to mastering the correct technical factors, the development of athletes' difficult movements is also closely related to whether they have the physical fitness level matched with the completion of the difficult movements [18].

Physical stamina is an important condition that determines the formation of technical movements, and the improvement of physical stamina is the basis for completing higher-level difficult movements. Special quality is an important condition that determines the formation of technical movements. Without the improvement of the level of special quality, it is impossible to complete higher levels of difficult movements. Every new development and every update of difficult movements is based on special physical quality. Based on the creation of corresponding athlete performance. Therefore, special physical fitness plays a vital role in the process of athletes completing a series of movements, and it is the basis and guarantee for athletes to complete difficult movements [19-20].

Performing gymnastics is a form of expression that specializes in sports culture and sports art using sports performances as artistic materials. Aerobics, cheerleading, sports dance, group gymnastics, recreational gymnastics, rhythmic gymnastics and other items of technical movements, costumes, props, music and other items constitute the main elements of performing gymnastics. The understanding of performing gymnastics in this study is to weaken its competitive nature, pay more attention to its performance, and make it more visible and entertaining [21-22].

Through artistic performance means to reflect the performance content and theme, through the display of the theme, deeply express its connotation, show the three-dimensional picture, let people experience its deeper influence, let people be on the scene. Through vivid body language to express the cultural connotation, music and clothing are often ignored by choreographers, only catering to the needs of the theme of the performance, to meet the needs of the performance [23]. Gymnastic movements are rich and colorful. Different levels have different movements and different difficulties. It is difficult for teachers to demonstrate every level or every set of movements, and the specifications of the movements they can do are not necessarily high. It is also impossible to remember every gymnastic theoretical knowledge, and there are troubles in the process of giving students demonstration and explanation [24].

2.3 Motion Capture

Different camera equipment and different shooting scenes will have different effects on the effect of image collection. Moreover, the image sensor will also have a greater impact on the results of the detection of moving human bodies. The choice of light source in the shooting scene will also have a direct impact on the image preprocessing process [25].

Using the one-dimensional center template, the expressions of the gradients in the x and y directions corresponding to the pixels at the position (x, y) are as follows [26].

$$G_x(x, y) = H(x+1, y) - H(x-1, y) \quad (9)$$

$$G_y(x, y) = H(x, y+1) - H(x, y-1) \quad (10)$$

Where H represents an image, H(x, y) represents the gray value of the image at the pixel point (x, y). The gradient value at the pixel (x, y) can be calculated by the following formula [27].

$$G(x, y) = \sqrt{G_x(x, y)^2 + G_y(x, y)^2} \quad (11)$$

The gradient direction of the pixel (x, y) in the sample is:

$$\theta(x, y) = \tan^{-1}\left(\frac{G_y(x, y)}{G_x(x, y)}\right) \quad (12)$$

The motion capture system based on MEMS sensors completely relies on inertial sensors for the collection of human motion data. In this way, when the human body is collected, the sensor must be installed on the moving limbs according to the captured part. This will inevitably cause There are many data collection and data transmission lines attached to the limbs of the human body during motion capture, which undoubtedly has an inevitable restriction on the movement of the human body [28].

The schematic diagram of human action capture is shown in Figure 2. Deploying the sensor nodes of the motion capture device on the human body is the basic link to achieve the effect of human motion capture. The location and number of sensor nodes deployed on the human body are directly related to the accuracy of action capture effect. According to different practical uses and needs, the accuracy required for human motion capture is also different, but when motion capture devices are used in medical rehabilitation, film and television production and other applications, the higher the accuracy, the better. The higher the accuracy is, the more sensor nodes are needed, so the more data flow is generated, and the more data the computer needs to calculate. As the central node, data sink node plays a role of data aggregation and transfer. The sink node reads the sensor data collected by each sensor node in a certain order, and packages it according to a certain format. The data sink node also has a wireless transmission module, which can send the packaged results to the computer terminal in real time. The upper computer program mainly realizes the operation of the sensor data sent by the sink node, which is used for the processing of sensor data and the synthesis of human body posture data. It drives the 3D human body model to make the same action with the user synchronously, and plays the role of a large number of sensor data operation and human body action simulation.

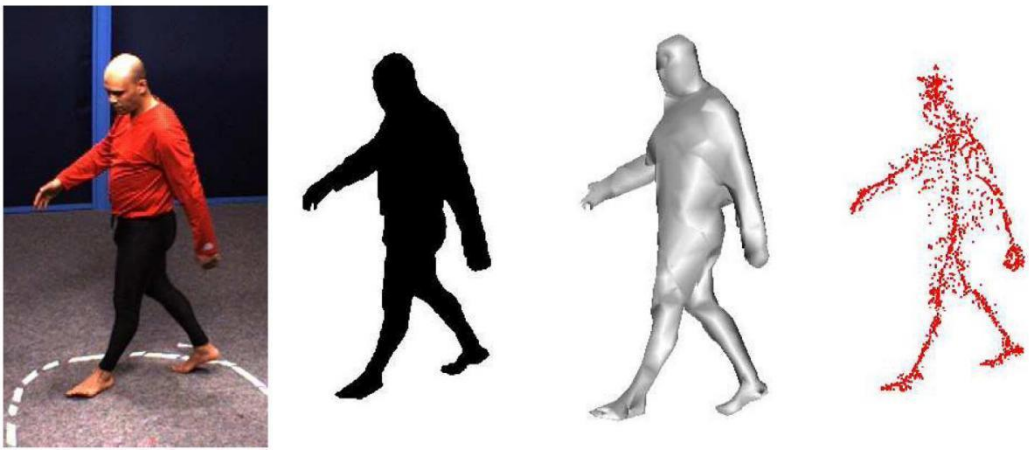

Figure 2. Schematic diagram of human motion capture (picture from http://alturl.com/2zcmc)

3. Gymnastics Performance Simulation Experiment

3.1 Sensor Parameter Setting

This article uses 3-DoFMEMS accelerometer and 3-DoFMEMS gyroscope. MPU-6000 uses three 16-bit ADCs to convert the analog signals measured by the accelerometer and gyroscope into digital signals that can be output. In order to accurately measure fast and slow motion, the measurement range of MPU-6000 is artificially controllable, the measurement range of the accelerometer is ±2g, ±4g, ±8g and ±16g; the measurement range of the gyroscope is ±250° /Sec (dps), ±500(dps), ±1000(dps) and ±2000(dps).

3.2 Sensor Data Preprocessing

In reality, the MEMS motion sensor is full of various interferences in the process of taking motion data. There is also noise interference in the acceleration signal transmission process. The jitter of the mobile device will also generate new noise, which makes the collected motion the sensor data contains not only the acceleration information of human behavior but also other interference information. Since the acceleration sensor signal collected when the human body is moving includes the noise part, the gravitational acceleration part and the behavior signal part of the actual human motion, the noise bandwidth of the accelerometer is much larger than the frequency bandwidth of the acceleration signal, and the high frequency signal is filtered out and the low frequency is retained. The signal can then remove noise. In the preprocessing to reduce noise interference, median filtering is mainly aimed at filtering and reducing noise of nonlinear signals, which can effectively remove signal glitches. The expression of the Butterworth low-pass filter is as follows:

$$\left|L(w)\right|^2 = \frac{1}{1+\left(\frac{\omega}{\omega_c}\right)^{2N}} = \frac{1}{1+\varepsilon^2\left(\frac{\omega}{\omega_p}\right)^{2N}} \quad (13)$$

In the formula, N is the order of the filter; ω_c is the cutoff frequency, that is, the frequency when the amplitude drops to -3db; ω_p is the edge frequency of the passband, which can be determined according to the spectral characteristics of the signal.

3.3 Motion Capture of Gymnastics Performance

In the experiment design of the motion capture device, the software used to display the effect of motion capture is Visual C + + 6.0 which is produced by Microsoft company. Using virtual character model to perform gymnastics. The computer receives sensor data from the sink node of the motion capture device through a Bluetooth communication module. The unit calculates the quaternion output from the dynamic link library of sensor data processing, calculates the rotation and coordinate offset of the limb where each sensor node is located, and realizes the real-time rendering of the virtual human model by using the driver of the human model. At the same time, it controls the storage of sensor data, the driving of model and the display of graphical interface. In the process of debugging and improving the algorithm of human motion capture, because the fusion process of sensor data has been encapsulated into a dynamic link library, the application directly calls the output of DLL. Therefore, if you need to adjust the data fusion processing algorithm, you only need to adjust the DLL of data processing without modifying the application.

3.4 Signal Acquisition

The gesture recognition system based on MEMS sensors uses a total of 14 MEMS sensors in a single hand to collect single-hand gesture signals. The node gesture signals of 14 sensors at the same time node constitute the complete gesture signal of the time node. Therefore, ensuring the synchronization of signal transmission and the consistency of transmission rate is the key to ensuring the accurate collection of gesture signals. The two IC data lines SDA and SCL interfaces of each BMI055 sensor module are connected to the multi-channel signal selection chip to ensure that the gesture signals of 14 MEMS sensors are obtained at the same time, so as to realize the collection and synthesis of the gesture signals of the key nodes of the hand into a complete gesture signal. When a

gesture action is about to occur, a trigger signal is given to the system to mark the beginning of the action, so as to obtain the initial data of each axis signal of the MEMS sensor. When the gesture action is completed, give the system a signal to end the action. Mark the end of the action, so that you can capture the original signal data during the beginning and end of the gesture action.

3.5 Communication Test

In order to ensure the normal communication between PS and PL, it is necessary to test the key interfaces involved. When the system is powered on and running, the AXIDMA core transmits the attitude information collected by the PL part to the DDR3SDRAM through the AXIHP bus. When the amount of data sent reaches the number 1MB set in AXIDMA, AXIDMA will generate an interrupt and send it to PS interrupt information. Then you can view the posture information received sequentially from the initial address 0x10300000 in the memeory window. Since the data received by the SPI acquisition module is irregular, it is impossible to verify whether the data is wrong, so replace the SPI acquisition module with a data that automatically increments. Module, and generate IP core, build a test platform for testing. After testing, the data transmission rate is 298MB/s, realizing high-speed data transmission. Data transmission is correct, AXIDMA realizes the correct communication between PS and PL.

4. Results and Discussion

4.1 Sensor Performance Analysis

The effect of magnetometer before and after compensation is shown in Figure 3. It can be seen from Figure 3 (a) that the fluctuation of the original X-axis data of the magnetometer without error compensation is as high as 720 μ T, and the fluctuation of the original X-axis data of the magnetometer after compensation is reduced to 50 μ T. According to Figure 3 (b), in 10 repeatability experiments, the output average fluctuation of the x-axis of the magnetometer is not large after compensation, and the output value of the x-axis of the magnetometer is near 911 μ T. The experimental results show that after error compensation, the magnetometer can enhance the stability of the magnetometer under the environment of magnetic interference and improve the anti noise capability of the magnetometer.

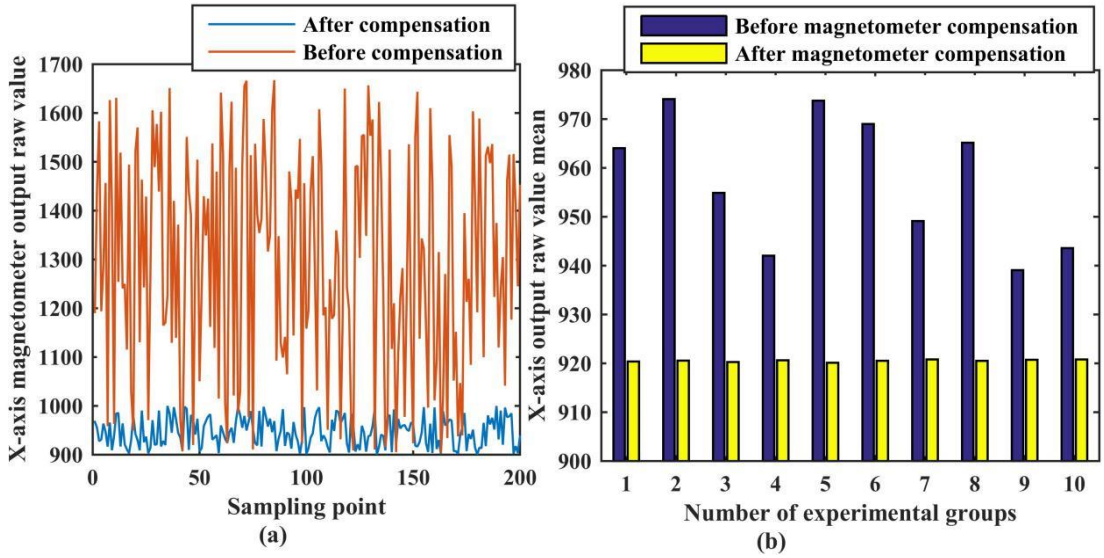

Figure 3. Effect before and after magnetometer compensation

The comparison of the weighted average coefficients corresponding to different recognizers is shown in Figure 4. From the correlation coefficients in the table, it can be found that the recognition

accuracy of the corresponding recognizers is from high to low in order: traditional decision tree recognizer, two-layer decision tree-based recognizer, Bayesian recognizer, support vector machine recognizer, but from the algorithm complexity of the system, the complexity based on the two-layer decision tree is absolutely reduced; and when the detected behavior appears stationary and walking that are common in daily behavior, the system is It only needs to extract the data of the gyroscope sensor without mentioning the data of the angular velocity sensor, so the energy consumption of the system is also greatly reduced.

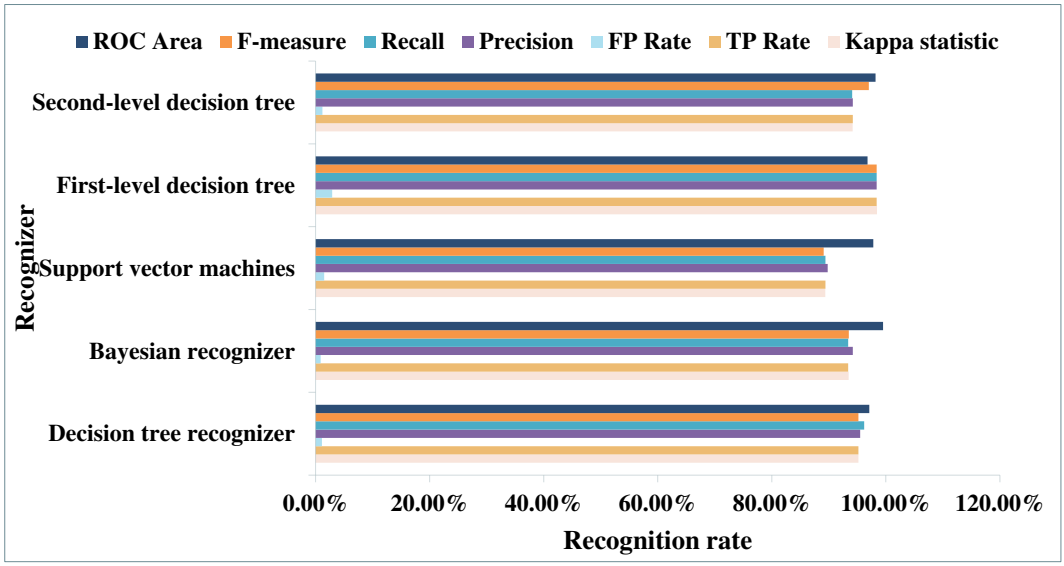

Figure 4. Comparison of weighted average coefficients corresponding to different recognizers

When the system is placed in a real measurement scenario, the system output is the dynamic output. Due to the effective filtering method, the stability of the dynamic output of the system will prove the effectiveness of the filtering. When the dynamic output tends to diverge, the algorithm is invalid, and when the dynamic output of the system tends to be stable, the algorithm is proved to be effective. The dynamic test results are shown in Table 1. It can be seen from the test results that after effective static data compensation and dynamic filtering, the posture display in this article starts from a certain position, and finally returns to the approximate original position, and the curve is smooth and complete. At the same time, when the more obvious external vibration is artificially added, the posture capture curve can be more clearly reflected and captured, and the dynamic characteristics are good.

Table 1. Dynamic test results

Resting time	Acceleration	Angular acceleration	Speed	Angular velocity
0.5	10	5	20	4
1	15	8	20	5
1.5	15	10	18	2
2	18	8	20	5
2.5	15	5	20	3
3	10	8	20	6

The experimental results of multi-level threshold detection are shown in Table 2. The results show that the specificity of the multi-level threshold detection method is relatively high, reaching 93.33%, indicating that the detection effect of normal behavior is better. The detection rates of jumping and running in daily behavior were both 85%. The detection rate of fall behavior was 91%, and the detection rate of lateral fall behavior was higher than that of before and after falls. Specifically, the

detection rate of lateral falls was 94%, and the detection rate of front and rear falls was 88%. The reason for this result is that when the human body falls back and forth, the cushioning effect of the hands before the human body collides with a low-power object is more significant than that of a lateral fall. The fall lead time of different fall and fall behaviors is slightly different, and the overall fall is between 0.28-0.35S. Among them, the lead time of a lateral fall is greater than that of a front-to-back fall.

Table 2. Experimental results of multi-level threshold detection

Test count	Number of warnings	No warning times	Average lead time
25	23	2	0.285
25	21	4	0.327
25	24	1	0.394
25	23	2	0.358

4.2 Action Simulation Results

The results of the system's three-dimensional space tracking experiment are shown in Figure 5. The average measurement error of X-axis displacement of the space tracking system is 8.17%, the average measurement error of Y-axis displacement is 7.51%, the average measurement error of Z-axis displacement is 9.72%, and the average error of three-dimensional space measurement is 8.7%. Compared with the magnetic space tracking system and the laser space tracking system, the error of the system is relatively large. In the magnetic and laser tracking system, the external reference system can improve the precise spatial coordinate position of the system. At the same time, their measurement range is also restricted by the external reference system. The space tracking system based on MEMS acceleration sensor breaks through the external restrictions and can realize free space measurement.

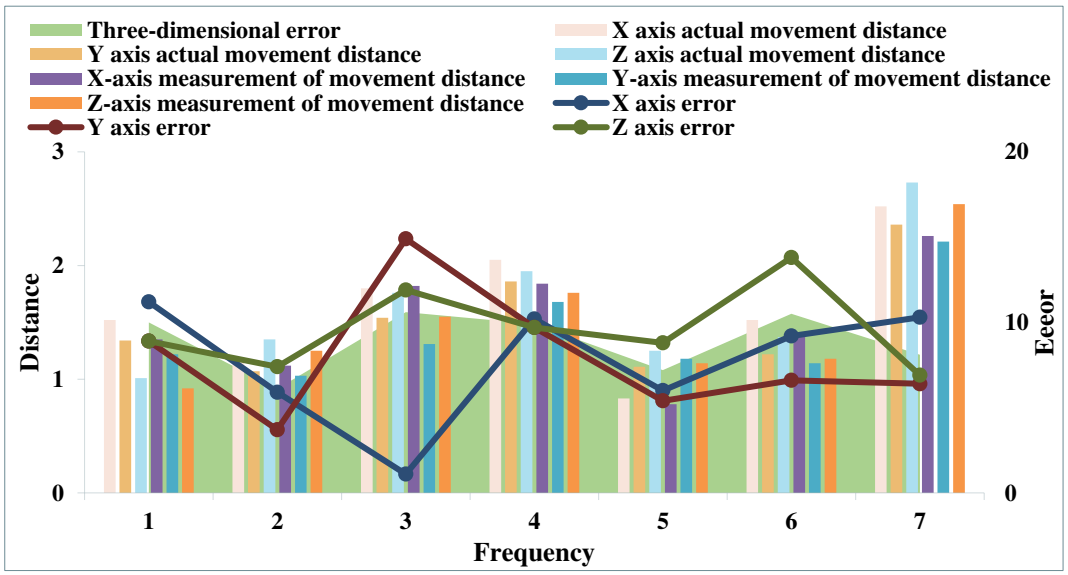

Figure 5. System three-dimensional space tracking experiment results

The data processing effect of the magnetoresistive sensor is shown in Table 3. From the experimental results, it can be seen that the rectified magnetoresistive sensor can accurately calculate the heading angle, and the error is within 1 degree, which can meet the accuracy requirements of human body motion capture.

Table 3. Data processing effect of magnetoresistive sensor

Actual angle	Measuring angle	Actual angle	Measuring angle
0°	0°	30°	30.71°
60°	59.84°	90°	90.52°
120°	120.62°	150°	150.18°
180°	180.26°	210°	209.83°
240°	239.51°	270°	269.01°
300°	299.25°	330°	329.69°

The average value of the pitch angle measurement angle is shown in Figure 6. When the given pitch angle of the three-axis turntable is within ±80 degrees, the pitch angle measurement error of the attitude measurement unit can basically be kept within 0.1 degrees, and then the measurement error increases slightly with the increase of the given pitch angle of the three-axis turntable. When the given pitch angle of the three-axis turntable increases to ±85 degrees, the measurement error rises to about 1 degree. When the given pitch angle of the three-axis turntable reaches around ±90 degrees, the measurement error drops slightly. In general, after the MEMS acceleration The pitch angle measurement accuracy of the attitude measurement unit after taking into account the calibration of the MEMS gyroscope can basically meet the measurement error of 0.1 degree. At the same time, the test result is the same as the result obtained by MATLAB simulation, indicating that the full-angle attitude estimation algorithm and attitude measurement given in this article are used. The equipment can realize the high-precision static measurement function of the pitch angle.

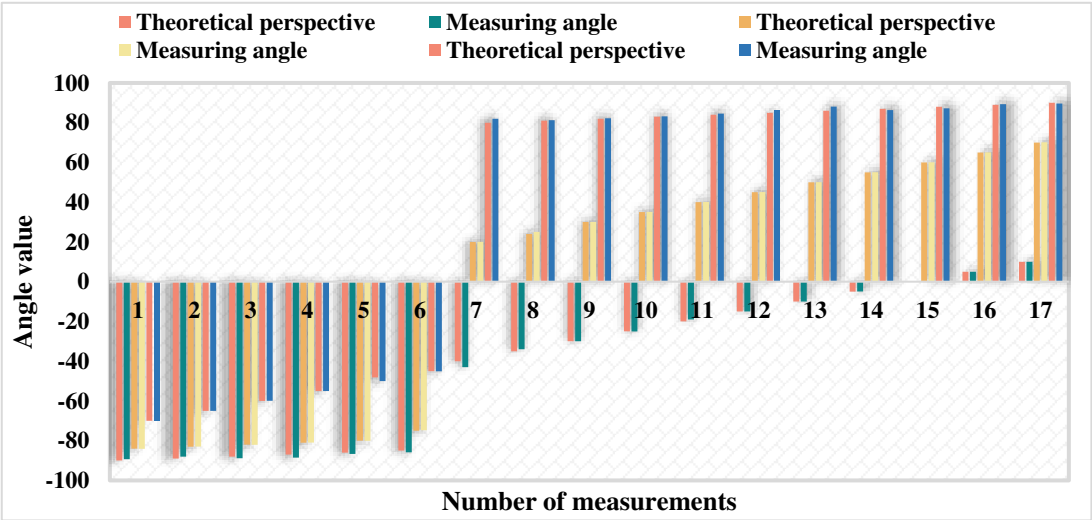

Figure 6. Average value of pitch angle measurement

Table 4 shows the calibration results of the accelerometer's zero offset and scale factor in different attitudes. After many experiments, statistics found that: the X-axis bias error can be reduced to 22.5mg, the scaling factor error is reduced to -0.15%~0.5%; the Y-axis bias error is reduced to 8.2mg, and the scaling factor error is 0.25%. Floating within the range of ~1.3%; the zero deviation error of the Z-axis can be reduced to 37.83mg, and the scale factor error is within the range of -1.85%~0.43%. The accuracy of the accelerometer zero offset and scale factor has been significantly improved.

Table 4. Accelerometer's zero offset and scale factor calibration results in different attitudes

	Datax	Datay	Dataz
Posture 1	-186.19	-8	1936
Posture 2	-23.619	-107	-2200
Posture 3	-19	-2021.3	-166

Posture 4	26.238	2038.6	-303
Posture 5	-2032	-44	-305
Posture 6	2101	-6.0952	-144

4.3 Sensor Error Analysis

Figure 7 shows the comparison before and after data processing of the acceleration sensor. After processing, the waveform output by the acceleration sensor only contains the fundamental signal and a small amount of low-frequency signals. On the surface, much of the effective information in the output signal of the acceleration sensor is lost, but in fact, the information lost here can be obtained from the angular velocity sensor in the subsequent complementary filtering process.

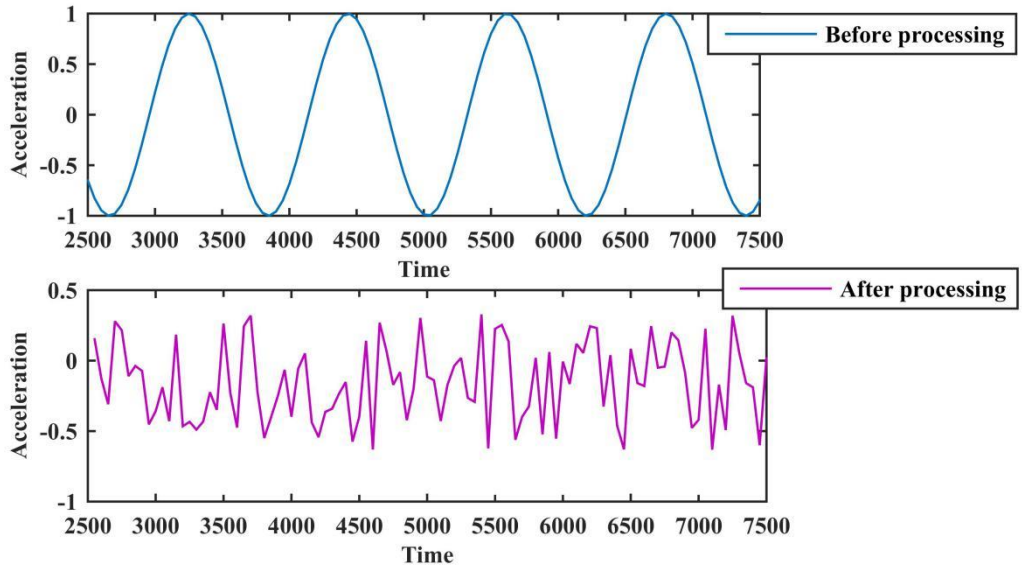

Figure 7. Acceleration sensor data processing before and after comparison

The performance index of motion recognition is shown in Figure 8. From the experimental results, the precision rate and recall rate indicators under several schemes did not deviate seriously, and the classification results of the model are credible. Further analysis of the experimental results shows that the feature-based recognition scheme in offline mode can achieve higher recognition accuracy and can flexibly adjust the feature combination according to actual needs; for online action recognition, the convolutional neural network algorithm can show that the data the robustness of the displacement, in fact, the translation expansion of the data set improves the recognition performance of the network, and does not need to greatly increase the training time. Therefore, the scheme based on deep learning can better cooperate with the simple sliding window sampling method to achieve action recognition.

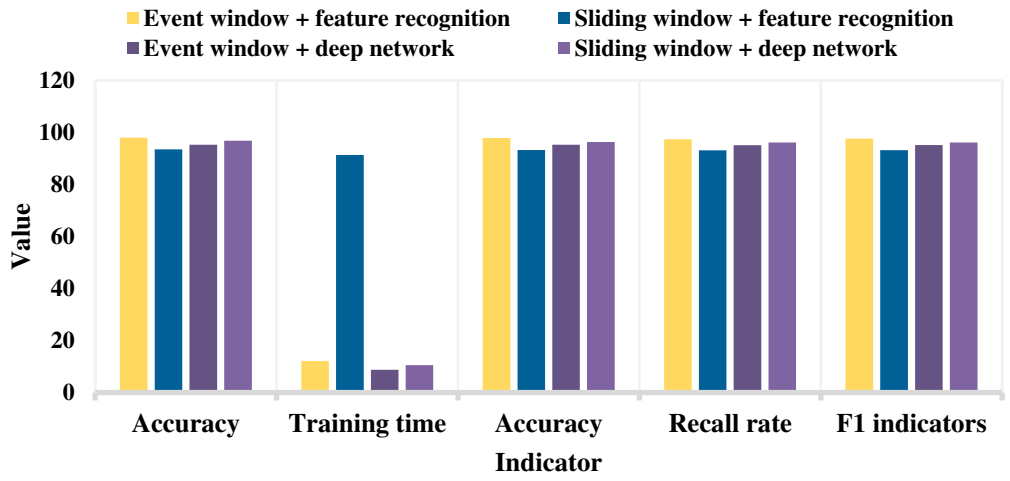

Figure 8. Performance indicators for motion recognition

The amplitude comparison before and after correction of the acceleration of gravity is shown in Table 5. The average output value of the actual accelerometer reaches 1.06g. After the static error correction is performed by the least squares method, the average output amplitude of the accelerometer becomes 0.957g, and the average amplitude error is reduced by 70% from the original value. The static error correction is performed by the ant colony algorithm. The average value of the corrected acceleration value is almost the same as the acceleration of gravity. The variance of the acceleration value after correction by the ant colony algorithm is reduced by 70% compared with the original data. The error correction effect is obvious, which also proves the effectiveness of the ant colony algorithm.

Table 5. Comparison of amplitude before and after correction of acceleration of gravity

Correction method	Amplitude average performance comparison		Standard deviation comparison of amplitude	
	Average value	Compared to the original	Variance	Compared to the original
Original value	1.056g	100%	0.094g	100%
Least squares method	0.957g	77.03%	0.056g	40%
ACO	1.002g	96.55%	0.029g	70%

The training and recognition results of the two-classification pattern are shown in Table 6. It can be seen from the table that SVC has excellent performance in the realization of two classification recognition. Not only does the CV accuracy rate reach 100% when all optimization algorithms are used, but the final recognition accuracy rate is also 100%, that is to say achieve complete recognition of the test set. However, the number of support vectors and parameter optimization results obtained in the training and optimization process are different. That is to say, the recognition accuracy has reached the maximum value, but the parameters c and g are not necessarily the best. In this case, it is impossible to analyze the pros and cons of the optimization algorithm and the performance of SVC. Therefore, the experimental research of multi-classification mode should be continued.

Table 6. Two-classification pattern training and recognition results

SVC	Support vector number			Parameter optimization result		Accuracy(%)		Duration (s)
11	1	2	Total	c	g	CV	Identify	
GS-SVC	20	20	40	0.0039	0.0039	100	100	0.54
GA-SVC	3	4	7	3.8369	0.4148	100	100	1.91

PSO-SVC	20	20	40	0.1	0.01	100	100	2.68

5.Conclusions

With people's increasing attention to sports and the concept of healthy life, the human movement information acquisition system based on MEMS has extremely important application value. People can use the system to get more professional movement guidance, prevent sports injury in the process of actively participating in sports, and combine the system with big data technology, it can realize more comprehensive function of motion information analysis. In this paper, the working principles of acceleration sensor, gyroscope and magnetic sensor based on MEMS technology are analyzed respectively. According to the working characteristics of the sensor, the low-pass filtering method is selected to complete the preprocessing of the sensor data. Then, the error models of the three sensors are analyzed, and the sensor data are calibrated to improve the data accuracy. According to the principle of micro inertial devices, the requirements of human motion capture are analyzed, and the experimental platform is built. The communication between electronic devices is realized by using CAN protocol. The problems of device wearing and motion limitation are solved by using XBee WiFi wireless communication technology.

DECLARATIONS

Ethics Approval and Consent to Participate

This article is ethical, and this research has been agreed.

Consent for Publication

The picture materials quoted in this article have no copyright requirements, and the source has been indicated.

Availability of Data and Material

Data sharing does not apply to this article because no data set was generated or analyzed during the current research period

Competing Interests

The authors declare that they have no competing interests

Funding

The author(s) received no financial support for the research, authorship, and/or publication of this article.

Authors' Contributions

Bingxin Chen: Writing – editing

Lifei Kuang: data analysis

Wei He: sampling method

ABBREVIATIONS

microelectromechanical system (MEMS)

acoustic vector sensor (AVS)

direction of arrival (DoA)

dynamic mechanical analysis (DMA)
the dual-axis scanning mirror assembly (TSAY)
line of sight (LOS)
memory protection unit (MPU)

References

[1] K Józef, Grzegorz S . Calibration of acoustic vector sensor based on MEMS microphones for DOA estimation[J]. Applied Acoustics, 2018, 141(12):307-321.

[2] Kim Y , Liu D , Lee H , et al. Investigation of Stress in MEMS Sensor Device Due to Hygroscopic and Viscoelastic Behavior of Molding Compound[J]. IEEE Transactions on Components Packaging & Manufacturing Technology, 2017, 5(7):945-955.

[3] Park D H , Shin S , Kim Y K . Module packaging effects on MEMS airbag sensor performance for automobiles[J]. Microelectronics Reliability, 2017, 79(12):328-335.

[4] Huang H , Zheng X , Weipeng L I . Design and feedforward control of large-rotation two-axis scan mirror assembly with MEMS sensor integration[J]. Chinese Journal of Aeronautics, 2019, 32(8):1912-1922.

[5] Veena N , Balachandra T C , Umesh S . Design, Simulation and Analysis of MEMS based Piezoresistive Cantilever sensor[J]. Materials today: proceedings, 2018, 5(4):10697-10703.

[6] Wang D F , Liu H , Li X , et al. Passive MEMS DC Electric Current Sensor: Part I—Theoretical Considerations[J]. IEEE Sensors Journal, 2017, 17(5):1230-1237.

[7] Jakobsen, Henrik, Aasmundtveit, et al. Identification and Elimination of Hygro-Thermo-Mechanical Stress-Effects in a High-Precision MEMS Pressure Sensor[J]. Journal of Microelectromechanical Systems: A Joint IEEE and ASME Publication on Microstructures, Microactuators, Microsensors, and Microsystems, 2017, 26(2):415-423.

[8] Liu S , Xu H , Xu D , et al. Modelling of resonant MEMS magnetic field sensor with electromagnetic induction sensing[J]. Solid-State Electronics, 2017, 132(6):91-98.

[9] And D S , Maheshkumar G . Wireless Mems-Based Accelerometer Sensor System for Structure Vibration and Post Defamation Monitoring[J]. Advances in computational sciences and technology, 2017, 10(11):3197-3204.

[10] Xu W , Ma S , Wang X , et al. A CMOS-MEMS Thermoresistive Micro Calorimetric Flow Sensor With Temperature Compensation[J]. Journal of Microelectromechanical Systems, 2019, 28(5):841-849.

[11] Wei Z , Zhang W , Liu W , et al. Attitude Theory and Experimental Research of Micro-aircraft Based on MEMS Sensor[J]. Yadian Yu Shengguang/Piezoelectrics and Acoustooptics, 2018, 40(4):516-520.

[12] F . Li, Tan X , Wang T . Robust Design of MEMS Sensor Based on Piezoelectric Bimorph Beam[J]. Yadian Yu Shengguang/Piezoelectrics and Acoustooptics, 2018, 40(1):33-37.

[13] Takamatsu H , Wang H , Fukunaga T , et al. Measurement of fluid thermal conductivity using a micro-beam MEMS sensor[J]. International Journal of Heat and Mass Transfer, 2018, 117(2):30-35.

[14] Wada Y , Nobunaga N , Kumagai S , et al. MEMS Resonator-Based Insulated Voltage Sensor Withstanding Higher Voltage[J]. Electrical Engineering in Japan, 2018, 203(1):239-244.

[15] Ganji B A , Kheiry S , Soleimani S . Design of small size and high sensitive less-invasive wireless blood pressure sensor using MEMS technology[J]. IET Circuits, Devices & Systems, 2019, 13(1):39-44.

[16] Okada N , Sasabuchi T , Koike K , et al. MEMS Magnetic Sensor with Bridge-Type Resonator and Magnetostrictive Thin Film[J]. Electronics & Communications in Japan, 2018, 101(3):90-95.
[17] Sandvand S , Halvorsen E , Aasmundtveit K E , et al. Identification and Elimination of Hygro-Thermo- Mechanical Stress-Effects in a High-Precision MEMS Pressure Sensor[J]. Journal of Microelectromechanical Systems, 2017, 26(2):415-423.
[18] Araki R , Abe T , Noma H , et al. Electromotive Manipulator Control by Detection of Proximity, Contact, and Slipping Using MEMS Multiaxial Tactile Sensor[J]. Electrical Engineering in Japan, 2018, 204(2):44-49.
[19] AA S Rabih, Dennis J O , Ahmed A Y , et al. MEMS-Based Acetone Vapor Sensor for Non-Invasive Screening of Diabetes[J]. Sensors Journal, IEEE, 2018, 18(23):9486-9500.
[20] Xu W , X Wang, Yi C , et al. High Sensitivity and Wide Dynamic Range Thermoresistive Micro Calorimetric Flow Sensor With CMOS MEMS Technology[J]. IEEE Sensors Journal, 2020, 20(8):4104-4111.
[21] Gerdroodbary M B , Anazadehsayed A , Hassanvand A , et al. Calibration of low-pressure MEMS gas sensor for detection of hydrogen gas[J]. International Journal of Hydrogen Energy, 2018, 43(11):5770-5782.
[22] Tallamraju R , Saini N , Bonetto E , et al. AirCapRL: Autonomous Aerial Human Motion Capture using Deep Reinforcement Learning[J]. IEEE Robotics and Automation Letters, 2020, 5(4):6678-6685.
[23] D'Amato V , Volta E , Oneto L , et al. Understanding Violin Players' Skill Level Based on Motion Capture: a Data-Driven Perspective[J]. Cognitive Computation, 2020, 12(1):1-14.
[24] Gao C Y , Wang B J , Feng M S , et al. Kinematic parameters and related influencing factors of sitting lumbar spine manipulation with motion capture[J]. Zhongguo gu shang = China journal of orthopaedics and traumatology, 2019, 32(9):802-806.
[25] Smith M . Shifting modes: Spectatorship, theatrical virtual reality and motion capture through the experience of Fatherland XR[J]. Virtual Creativity, 2019, 9(1):43-61.
[26] Kwolek B , Michalczuk A , Krzeszowski T , et al. Calibrated and synchronized multi-view video and motion capture dataset for evaluation of gait recognition[J]. Multimedia Tools and Applications, 2019, 78(22):32437-32465.
[27] Mueller F , Deuerlein C , Koch M . Intuitive Welding Robot Programming via Motion Capture and Augmented Reality - ScienceDirect[J]. IFAC-PapersOnLine, 2019, 52(10):294-299.
[28] Wan, Mohd, Rizhan, et al. A systematic survey of martial art using motion capture technologies: the importance of extrinsic feedback[J]. Multimedia tools and applications, 2019, 78(8):10113–10140.

Bingxin Chen was born in Kaifeng, Henan Province. China, 1988. She received a master's degree from the School of physical Education of Hunan normal University and worked at Hunan normal University. her research interests include physical education, sports management, sports training, and sports medicine.
E-mail: chenbingxin15@163.com

Lifei Kuang, born in 1979, graduated from Hunan normal University School of physical Education, Master's degree, Lecturer, Gymnastics International referee,

research field: physical Education and training
E-mail: lifekuang1@163.com

Wei He, born in Ningxiang, Hunan Province, 1986, China, obtained a master's degree in physical Education College of Hunan normal University, and now works in physical Education College of Changsha normal University.
E-mail: ccsbb@163.com

Figures

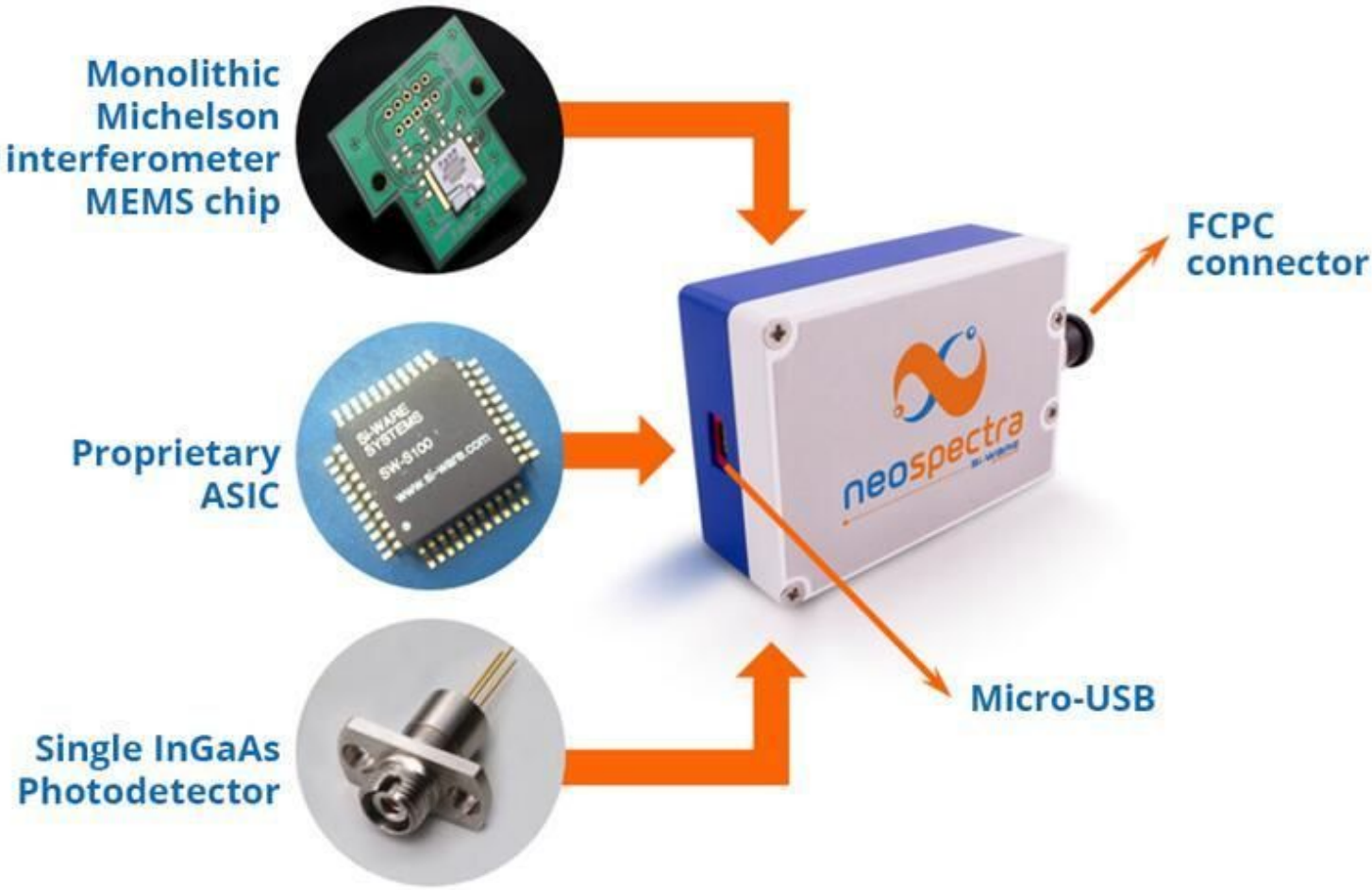

Figure 1

Physical image of MEMS sensor (picture from http://alturl.com/6ve7q)

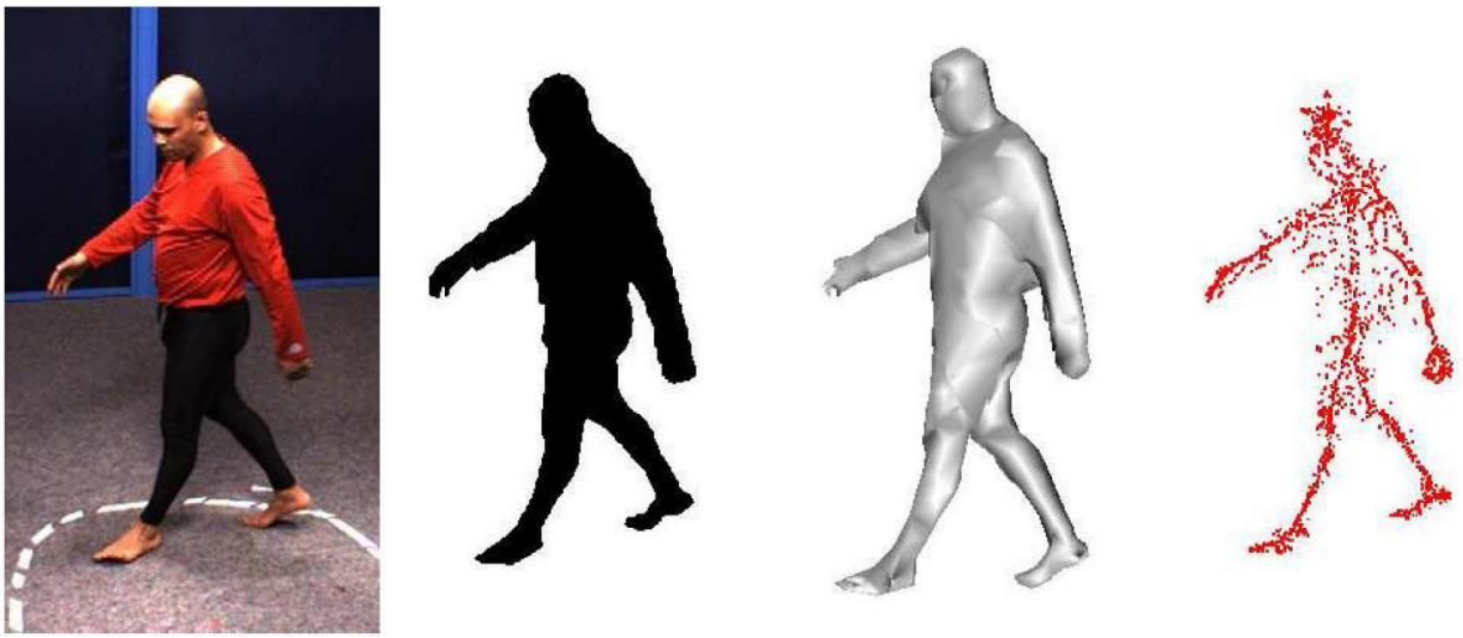

Figure 2

Schematic diagram of human motion capture (picture from http://alturl.com/2zcmc)

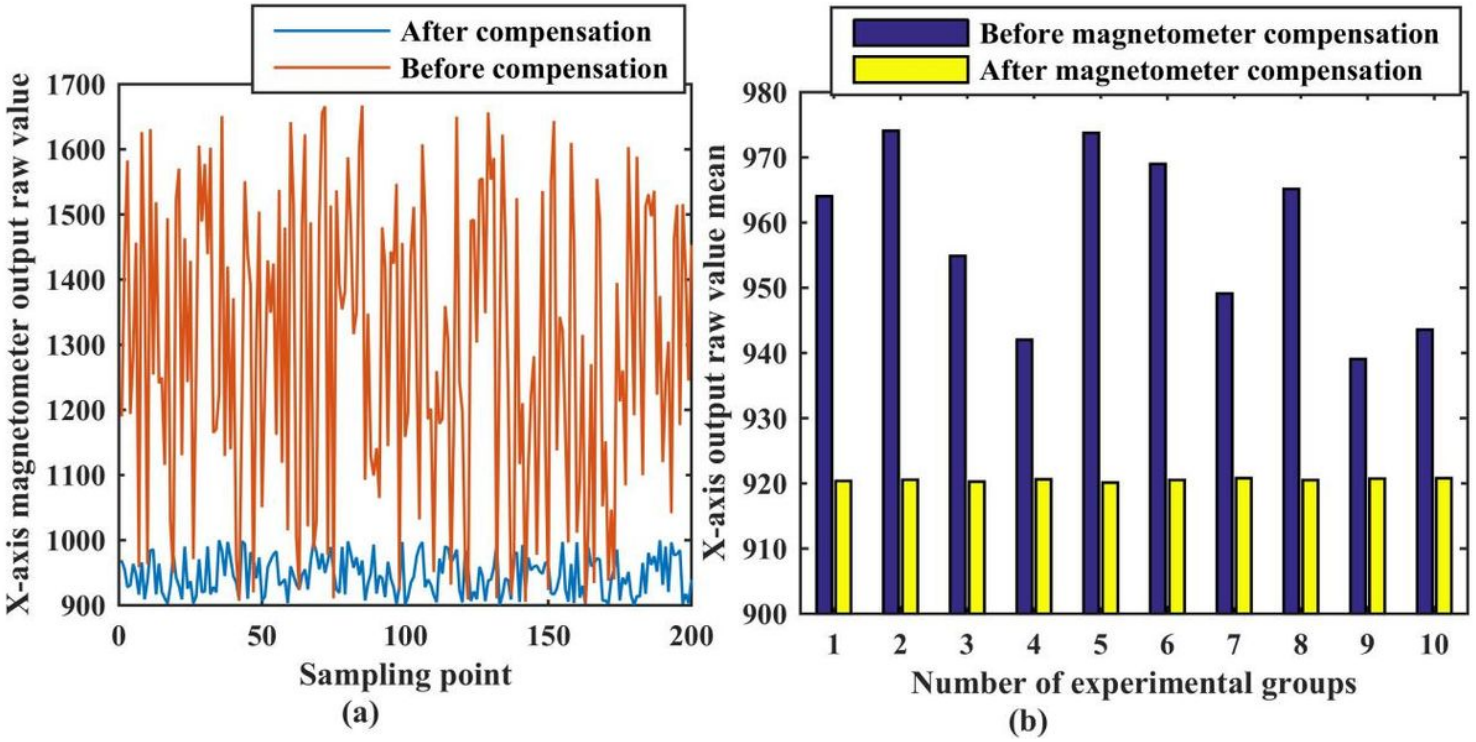

Figure 3

Effect before and after magnetometer compensation

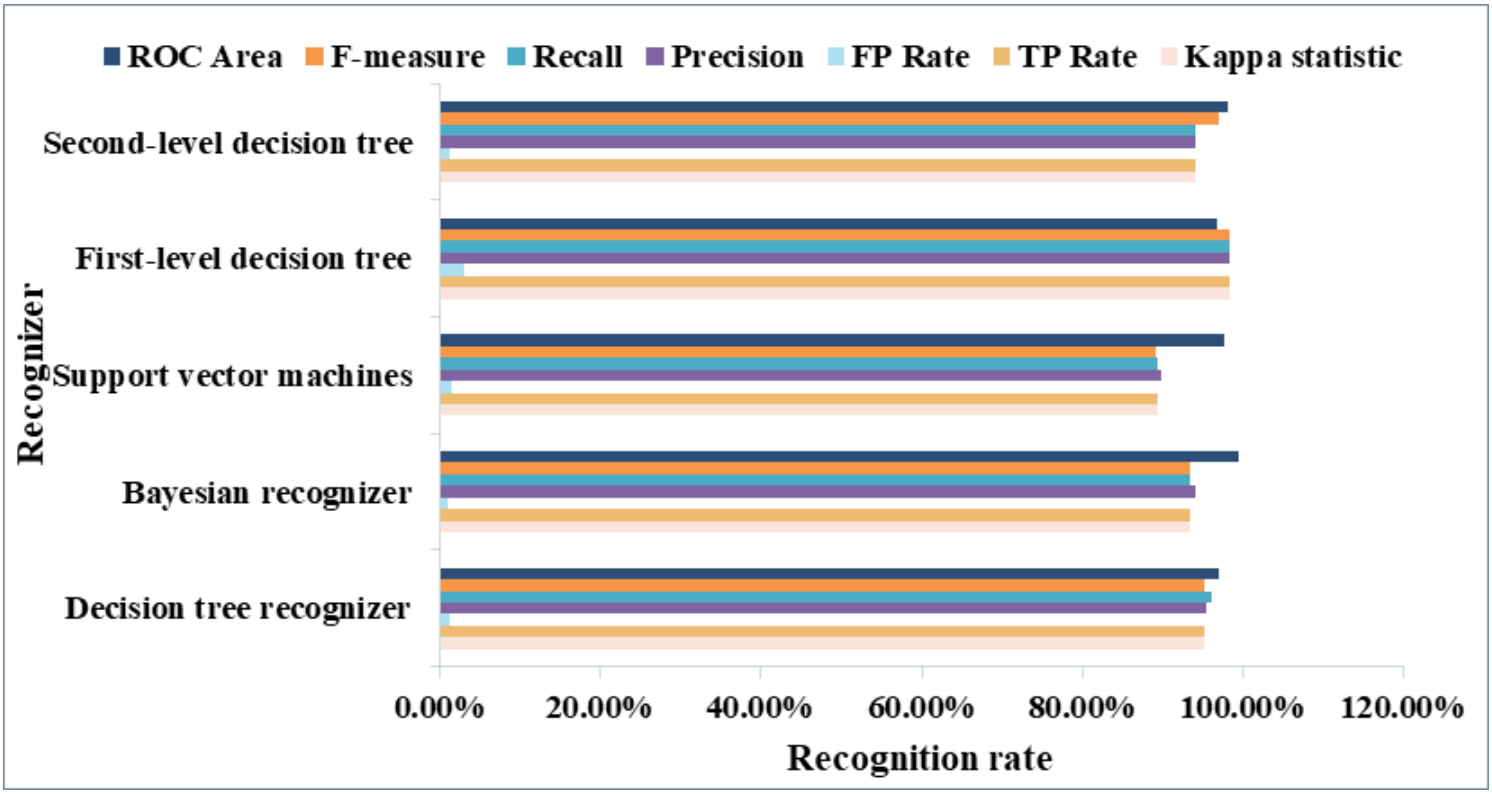

Figure 4

Comparison of weighted average coefficients corresponding to different recognizers

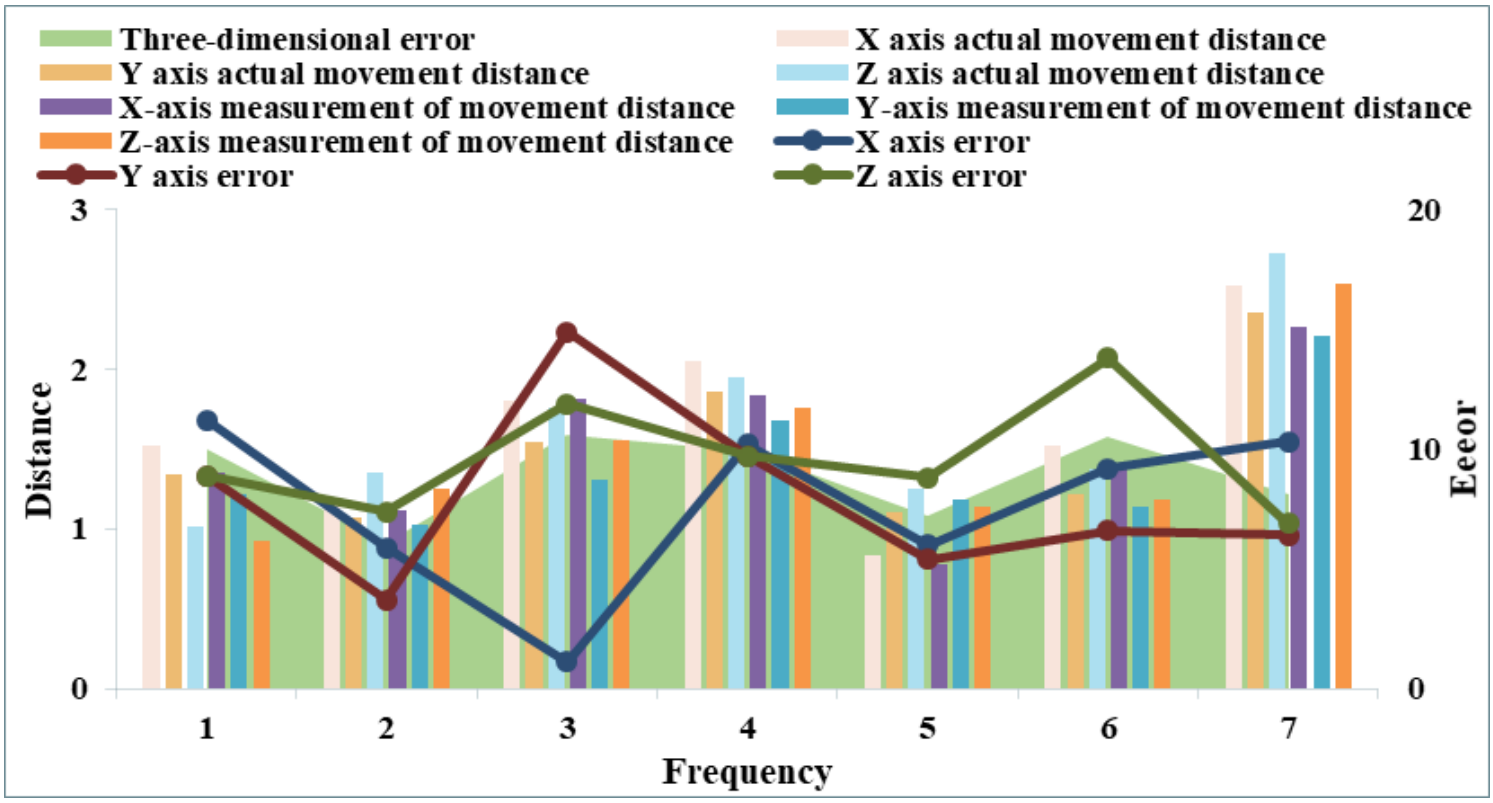

Figure 5

System three-dimensional space tracking experiment results

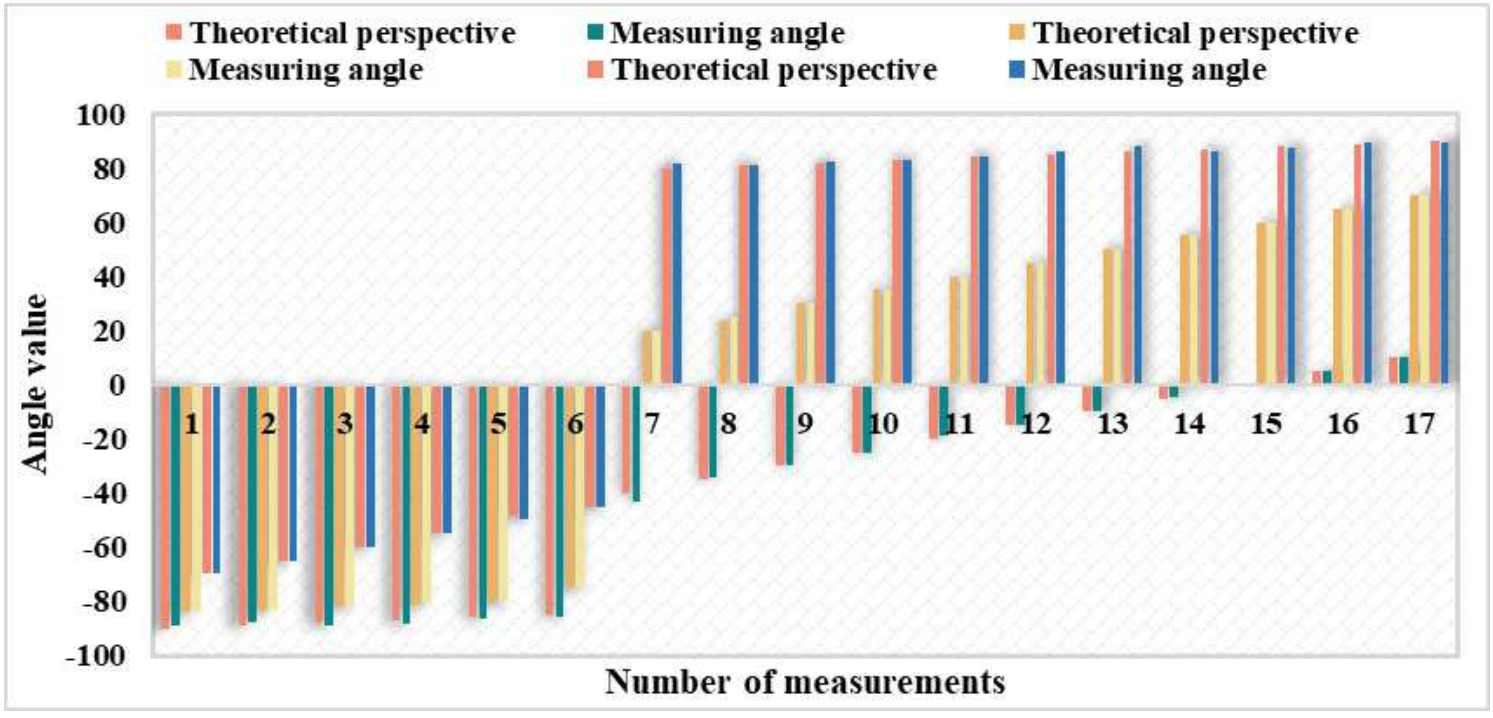

Figure 6

Average value of pitch angle measurement

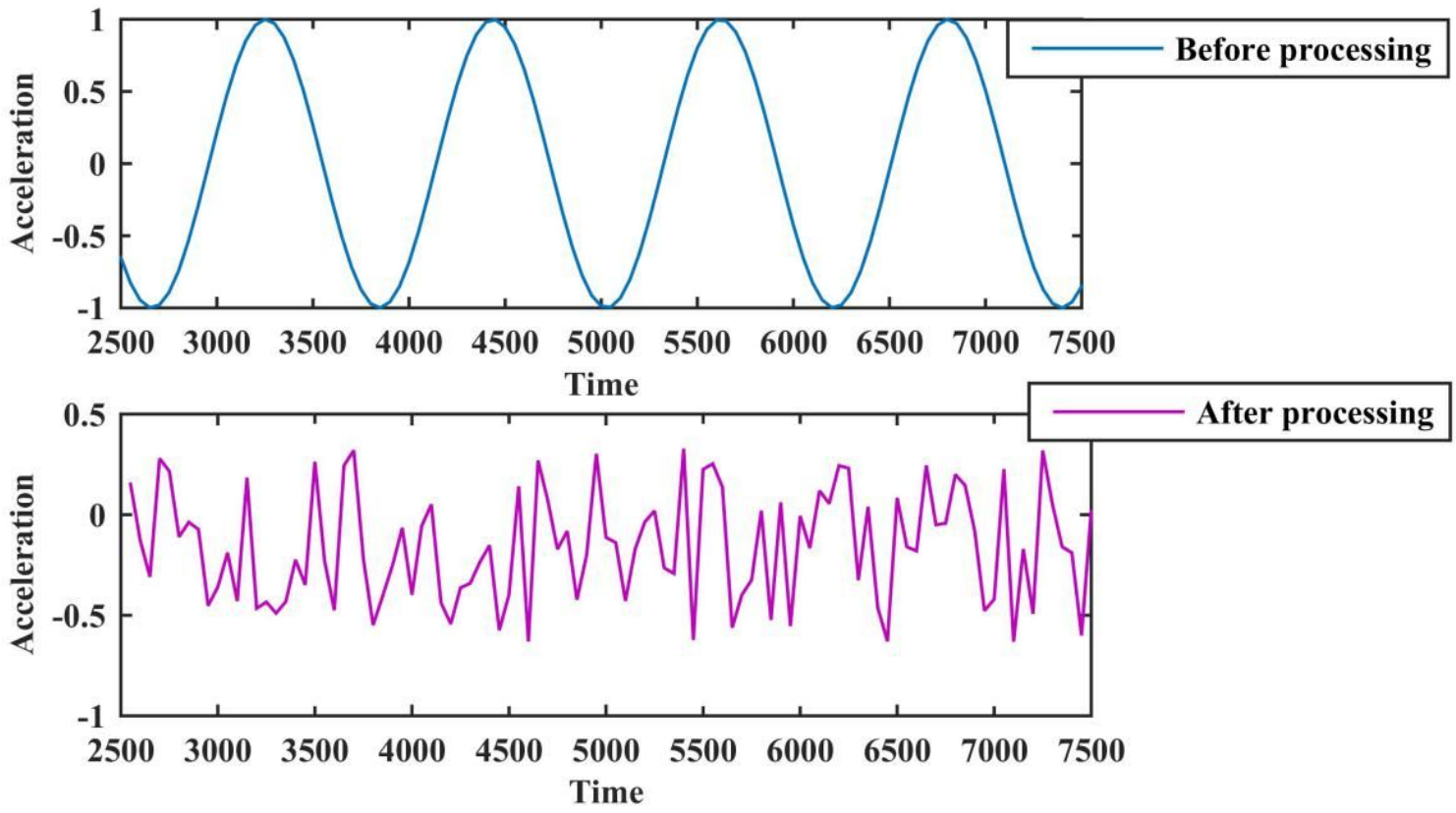

Figure 7

Acceleration sensor data processing before and after comparison

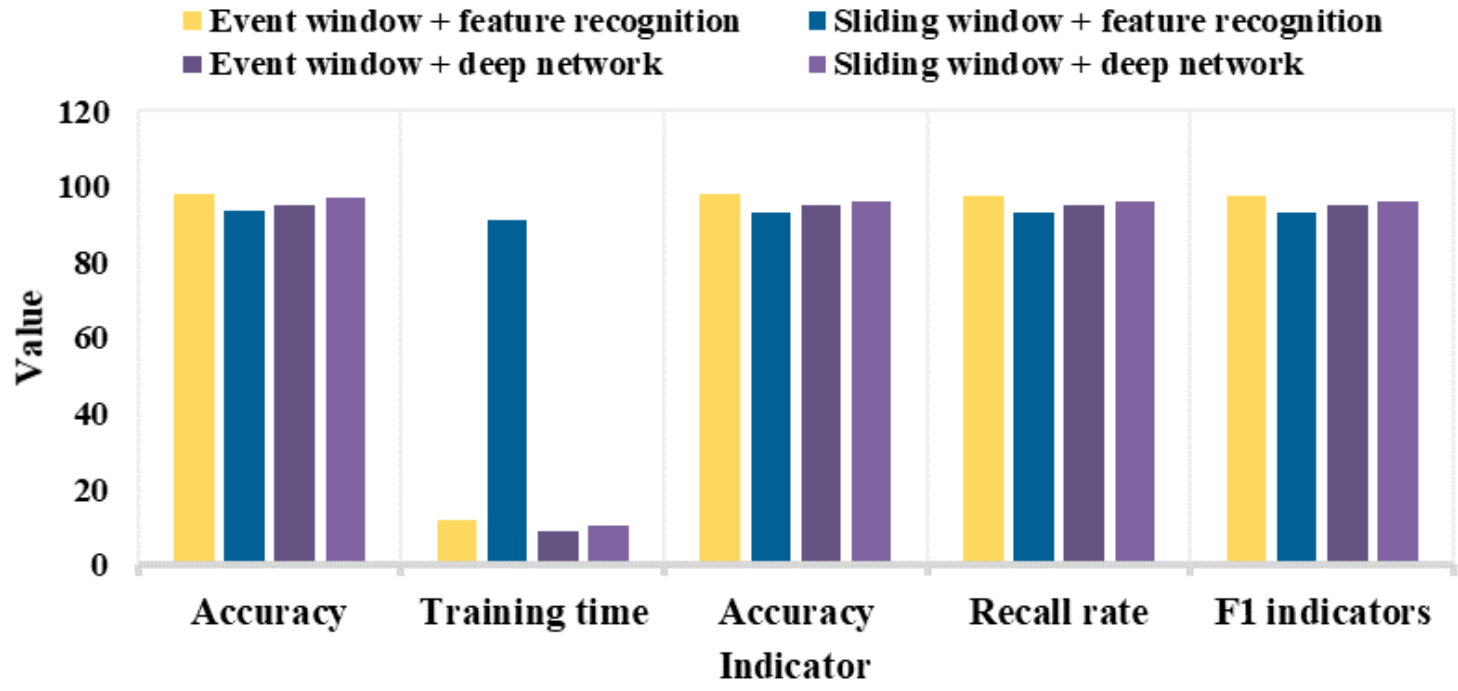

Figure 8

Performance indicators for motion recognition